Analysis of Myoglobin Adsorption to Cu(II)−IDA and Ni(II)−IDA Functionalized Langmuir Monolayers by Grazing Incidence Neutron and X-ray Techniques

M. S. Kent,* H. Yim, and D. Y. Sasaki

Department 1851, Sandia National Laboratories, Albuquerque, New Mexico 87185

S. Satija

NIST Center for Neutron Research, National Institute of Standards and Technology, Gaithersburg, Maryland 20899

J. Majewski

Los Alamos Neutron Science Center, Los Alamos National Laboratory, Los Alamos, New Mexico 87545

T. Gog

Advanced Photon Source, Argonne National Laboratory, Argonne, Illinois 60439

Received November 24, 2003

The adsorption of myoglobin to Langmuir monolayers of a metal-chelating lipid in crystalline phase was studied using neutron and X-ray reflectivity (NR and XR) and grazing incidence X-ray diffraction (GIXD). In this system, adsorption is due to the interaction between chelated divalent copper or nickel ions and the histidine moieties at the outer surface of the protein. The binding interaction of histidine with the Ni−IDA complex is known to be much weaker than that with Cu−IDA. Adsorption was examined under conditions of constant surface area with an initial pressure of 40 mN/m. After ∼12 h little further change in reflectivity was detected, although the surface pressure continued to slowly increase. For chelated Cu^{2+} ions, the adsorbed layer structure in the final state was examined for bulk myoglobin concentrations of 0.10 and 10 μM. For the case of 10 μM, the final layer thickness was ∼43 Å. This corresponds well to the two thicker dimensions of myoglobin in the native state (44 Å × 44 Å × 25 Å) and so is consistent with an end-on orientation for this disk-shaped protein at high packing density. However, the final average volume fraction of amino acid segments in the layer was 0.55, which is substantially greater than the value of 0.44 calculated for a completed monolayer from the crystal structure. This suggests an alternative interpretation based on denaturation. GIXD was used to follow the effect of protein binding on the crystalline packing of the lipids and to check for crystallinity within the layer of adsorbed myoglobin. Despite the strong adsorption of myoglobin, very little change was observed in the structure of the DSIDA film. There was no direct evidence in the XR or GIXD for peptide insertion into the lipid tail region. Also, no evidence for in-plane crystallinity within the adsorbed layer of myoglobin was observed. For 0.1 μM bulk myoglobin concentration, the average segment volume fraction was only 0.13 and the layer thickness was ≤25 Å. Adsorption of myoglobin to DSIDA-loaded with Ni^{2+} was examined at bulk concentrations of 10 and 50 μM. At 10 μM myoglobin, the adsorbed amount was comparable to that obtained for adsorption to Cu^{2+}-loaded DSIDA monolayers at 0.1 μM. But interestingly, the adsorbed layer thickness was 38 Å, substantially greater than that obtained at low coverage with Cu−IDA. This indicates that either there are different preferred orientations for isolated myoglobin molecules adsorbed to Cu−IDA and Ni−IDA monolayer films or else myoglobin denatures to a different extent in the two cases. Either interpretation can be explained by the very different binding energies for individual interactions in the two cases. At 50 μM myoglobin, the thickness and segement volume fraction in the adsorbed layer for Ni−IDA were comparable to the values obtained with Cu−IDA at 10 μM myoglobin.

I. Introduction

The interaction of biomacromolecules with lipid membranes is of great interest in many areas, including drug discovery, understanding cellular signaling, combating biowarfare agents, and the development of sensor materials. From a fundamental point of view, a general goal is to understand how various types of fundamental interactions, and their spatial distribution, affect the conformation, orientation, and extent of aggregation (in-plane and out-of-plane of the lipid membrane) of an adsorbed protein. The orientation of an enzyme, for example, can affect access to its active site, and thus activity. Another important question is what conditions lead to denaturation upon adsorption to the membrane surface. In bulk solution, myoglobin has been shown to unfold at ambient pressure at 74 °C at pH 7.6, and at much lower temperatures at elevated pressures.[1] Myoglobin has also been found to unfold at pH 3.9 at ambient temperature and pressure[2,3] and even to form fibrils in the presence of sodium borate at pH 9.0 at 65 °C.[4] It is important to know whether significant conformational changes may occur upon strong adsorption to a substrate as well. The extent of penetration of protein segments into lipid membranes is a further topic of interest, particularly important for understanding the mechanisms by which toxins enter cells. Finally, it is important to understand the factors that control the ability of an ensemble of adsorbed proteins to sample the

(1) Smeller, L.; Rubens, P.; Heremans, K. *Biochemistry* **1999**, *38*, 3816.

(2) Bergers, J. J.; Vingerhoeds, M. H.; van Bloois, L.; Herron, J. N.; Janssen, L. H. M.; Fischer, M. J. E.; Crommelin, D. J. A. *Biochemistry* **1993**, *32*, 4641.

(3) Puett, D. *J. Biol. Chem.* **1973**, *248*, 4623.

10.1021/la036207y CCC: $27.50
Published on Web 02/07/2004

configuration space and attain the minimum free energy state and the time scales involved. This is clearly related to the strength of the binding interaction as well as the mobility of the lipids. Indeed, two-dimensional (2-D) crystals of proteins have only been reported to form underneath lipid monolayers in the fluid phase.[5−7] The present work corresponds to a rather constrained system involving a lipid in the crystalline phase at relatively high surface pressure and a strong protein−lipid binding interaction.

In this work we examine protein adsorption to lipid monolayer films using grazing incidence X-ray and neutron techniques to gain new insights into some of these questions. For biomimetic studies, lipid membranes at fluid−fluid interfaces offer the advantage of in-plane mobility of the lipids, mimicking aspects of cell membranes. This can be accomplished using either lipid monolayers at the liquid−air interface or lipid bilayers in the form of vesicles or supported on a solid substrate with a hydrated layer in between. These systems are complementary. Whereas lipid bilayers more closely resemble the structure of a cell membrane, Langmuir monolayers can provide insight into the free energy of interaction within the lipid/protein layer through the surface pressure of the films. Studies of protein adsorption to lipid monolayers at the liquid−air interface have involved mainly surface pressure isotherms, ellipsometry, and fluorescence and Brewster angle microscopies,[8−13] with much of the work focusing on lipid reorganization and protein−protein interactions in the two-dimensional plane. Regarding protein adsorption to lipid bilayers, adsorbed amounts have been obtained by depletion experiments via centrifugation of protein-bound vesicles[14] or qualitatively estimated using AFM imaging on supported lipid bilayers. More detailed structural information is needed to provide deeper insight into the mode of protein interaction with lipid films. Information regarding protein orientation, potentially subtle conformational changes, the extent of penetration into the lipid layer, and the extent of crystallinity within both lipid and protein layers would provide finer detail of the molecular-level interactions in these host−guest complexation systems.

Neutron and X-ray reflection (NR and XR, respectively) along with grazing incidence X-ray diffraction (GIXD) form a powerful combination for examining these questions. NR and XR are complementary techniques that probe the structure of the lipid−protein system normal to the interface in-situ and noninvasively. Each addresses certain questions more effectively than the other. Whereas both techniques have some degree of sensitivity to both lipid and protein layers, the contrast is much more favorable for detecting the protein in NR and the accessible q_z-range and contrast are more suitable for probing the lipid layers in XR. GIXD yields information on in-plane crystalline structure. In the present system, crystalline structure arises from the packing of the lipid tails. By monitoring the diffraction peak as well as XR during the adsorption process, the effect of protein binding on the structure and the in-plane phase behavior of the lipid film can be examined.

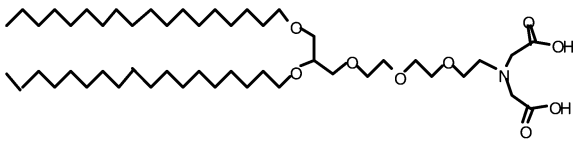

DSIDA

Figure 1. Chemical structure of the synthetic IDA-functionalized lipid used in this work.

Here we apply these methods to analyze a model system involving myoglobin adsorption to Langmuir monolayers of metal affinity ligands. The metal ion chelating lipid is DSIDA, shown in Figure 1, which has an iminodiacetate headgroup and two saturated aliphatic tails. The use of metal ion coordination to target the adsorption of proteins to lipid membranes has been studied extensively by others.[8−12,14−18] This method utilizes coordination interactions between metal ions and naturally occurring histidine units, genetically engineered metal ion binding sites, or polyhistidine units inserted at either the N or C terminus of proteins. Whereas in principle a number of functional groups participate in metal binding, it has been shown that the side chains of histidine dominate protein binding to chelated Cu^{2+}, Ni^{2+}, Zn^{2+}, Co^{2+}.[15,20] This versatile method provides a strategy for selectively targeting proteins for adsorption, for orienting proteins at engineered interfaces, and for 2-D crystallization. In the present context, Langmuir monolayers of such lipids form a flexible and well-defined model system in that a variety of metal ions can be used to tailor the strength of the interaction and the areal density of interaction sites can be precisely controlled. In addition, either the pressure or the area per molecule can be imposed and varied systematically to understand the effects of pressure on the interaction of amino acid segments with the membrane. Moreover, the role of specific versus nonspecific interactions can be elucidated using lipid mixtures. In addition to serving as a model system for protein adsorption, metal-affinity systems have practical importance as well, such as in protein separation and purification technologies.[15] Furthermore, mixtures of metal-chelating lipids with other lipids are being investigated for sensor applications, as protein adsorption can lead to in-plane reorganization of the lipids detectable by fluorescence techniques.[10,11]

Myoglobin was chosen because its native structure is known in great detail and its interaction with Cu−IDA complexes has been studied previously by other methods.[14] A schematic of the structure of myoglobin is shown in Figure 2.[21] Eight α-helices comprise more than 75% of the

(4) Fandrich, M.; Fletcher, M. A.; Dobson, C. M. *Nature* **2001**, *410*, 165.
(5) Haas, H.; Brezesinski, G.; Mohwald, H. *Biophys. J.* **1995**, *68*, 312.
(6) Lenne, P. F.; Berge, B.; Renault, A.; Zakri, C.; Venien-Bryan, C.; Courty, S.; Balavoine, F.; Bergsma-Schutter, W.; Brisson, A.; Grubel, G.; Boudet, N.; Konovalov, O.; Legrand, J. F. *Biophys. J.* **2000**, *79*, 496.
(7) Courty, S.; Lebeau, L.; Martel, L.; Lenne, P. F.; Balavoine, F.; Dischert, W.; Konovalov, O.; Mioskowski, C.; Legrand, J. F.; Venien-Bryan, C. *Langmuir* **2002**, *18*, 9502.
(8) Venien-Bryan, C.; Lenne, P. F.; Zakri, C.; Renault, A.; Brisson, A.; Legrand, J. F.; Berge B. *Biophys. J.* **1998**, *74*, 2649.
(9) Dietrich, C.; Boscheinen, O.; Scharf, K. D.; Schmitt, L.; Tampe, R. *Biochemistry* **1996**, *35*, 1100.
(10) Maloney, K. M.; Shnek, D. R.; Sasaki, D. Y.; Arnold, F. H. *Chem. Biol.* **1996**, *3*, 185.
(11) Pack, D. W.; Ng, K.; Maloney, K. M.; Arnold; F. H. *Supramol. Sci.* **1997**, *4*, 3.
(12) Frey, W.; William R. Schief, J.; Pack, D. W.; Chen, C.-T.; Chilkoti, A.; Stayton, P.; Vogel, V.; Arnold, F. H. *Proc. Natl. Acad. Sci.* **1996**, *93*, 4937.
(13) Wang, S.-W.; Robertson, C.; Gast, A.; Koppenol, S.; Edwards, T.; Vogel, V.; Stayton, P. *Langmuir* **2000**, *16*, 5199.
(14) Shnek, D. R.; Pack, D. W.; Sasaki, D. Y.; Arnold, F. H. *Langmuir* **1994**, *10*, 2382.
(15) Arnold, F. H. *Biotechnology* **1991**, *9*, 151.
(16) Mallik, S.; Johnson, R. D.; Arnold, F. H. *J. Am. Chem. Soc.* **1994**, *116*, 8902.
(17) Ng, K.; Pack, D. W.; Sasaki, D. Y.; Arnold, F. H. *Langmuir* **1995**, *11*, 4048.
(18) Bischler, N.; Balavoine, F.; Milkereit, P.; Tschochner, H.; Mioskowski, C.; Schultz, P. *Biophys. J.* **1998**, *74*, 1522.
(19) Wilson-Kubalek, E. M.; Brown, R. E.; Celia, H.; Milligan, R. A. *Proc. Nat. Acad. Sci.* **1998**, *95*, 8040.
(20) Sulkowski, E. *BioEssays* **1989**, *10*, 170.

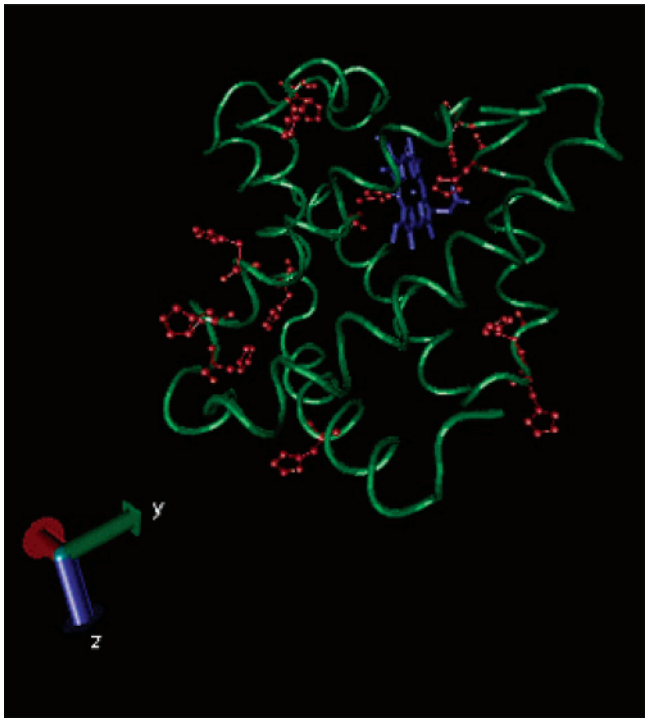

Figure 2. Schematic representation of the structure of myoglobin. The histidine units are indicated in red.

amino acid sequence. The mean charge is 0 at pH 7.3.[2] The dimensions calculated from the crystal structure are 44 Å × 44 Å × 25 Å.[2] It has 11 histidine units of which five are on the outer exposed surface and readily able to interact with the lipid film.[14,22] The histidine units are indicated in red in Figure 2. The Cu−IDA complex binds to histidine with an average binding constant of 4.5×10^3 M^{-1}, which corresponds to 4.8 kcal/mol or ∼8 kT.[23] This is about five times greater than the interaction energy for hydrogen bonding, is comparable to the interaction energy reported for a zwitterion-terminated polystyrene chain interacting with a mica surface (6−8 kT),[24,25] but is much less than the interaction energy for thiols on gold (∼170 kT) or trichlorosilanes on silicon oxide (∼320 kT).[26] Studies have shown that multipoint attachment results in apparent protein binding constants greater than 10^6 M^{-1}.[16] A lower limit for the binding constant of myoglobin to Cu−IDA complexes of $K_a > 2.9 \times 10^6$ M^{-1} was obtained by fitting a Langmuir isotherm to data for adsorption to liposomes.[14] This indicates that myoglobin interacts with Cu-loaded DSIDA films through multiple histidine residues. The adsorption data indicate that an adsorption plateau occurs for concentrations of free myoglobin greater than about 2 μM. In the present work, myoglobin concentrations of 10 and 0.1 μM were used to examine the structure of the adsorbed layer on the plateau as well as far below the plateau. The affinity of hystidine for Cu−IDA is 15 times that for Ni−IDA.[15] For Ni-loaded DSIDA, bulk myoglobin concentrations of 50 and 10 μM were used, which also span a wide range of adsorbed amount.

Recently, several studies probing the detailed structure of proteins bound to functionalized lipid monolayer films using grazing incidence X-ray and neutron techniques have been reported. These systems involve a wide range of interaction energy, allowing insightful comparisons with the present data. Losche et al. demonstrated the power of NR in examining the conformation of streptavidin adsorbed to monolayers of biotin-functionalized lipids and binary lipid mixtures.[27] XR and GIXD have been used to examine 2-D protein crystals formed upon adsorption to lipid monolayers[5−7] and the effect of the binding of a lung surfactant specific protein SP-B on the structure of palmitic acid monolayers.[28] Naumann et al. used NR to study the adsorption of hisactophilin (HIS) to mixed monolayers of dimyristoyl phosphatidylcholine (DMPC) and dimyistoyl phosphatidylglycerol (DMPG).[29] Natural HIS has a myristic acid chain at the N-terminus that is believed to serve as a membrane anchor. The authors studied the role of electrostatic interactions in the adsorption process, the insertion of protein segments into the lipid layer, and the effect of the orientation of adsorbed hisactophilin on the subsequent adsorption of actin. Their results showed that HIS adsorbed in single layers, and the area fraction covered with HIS ranged from 0.04 to 0.35 as the fraction of charged lipid increased from 0 to 0.5. This demonstrated the prominent role of electrostatic interactions in the adsorption, and that the presence of the myristic acid anchor alone was not sufficient to drive adsorption. The NR data provided strong evidence of the penetration of HIS into the lipid headgroup region. Their data were also consistent with a small amount of insertion of the myristic acid group into the lipid tail region, although this weak effect was at the limit of the uncertainty in the data. Maierhofer et al. studied the adsorption of cytochrome *c* to mixed monolayers of dipalmitoyl phosphatidylcholine (DPPC) and DMPG as a function of the mixed lipid phase state.[30] Their data indicated adsorption of single layers of cytochrome *c* in all cases. They also reported a strong increase in the adsorbed amount with increased fraction of charged lipid. Their results further indicated that domain formation can impact cytochrome *c* binding by enhancing the local concentration of charged lipids.

Below we report a study of structural characteristics of myoglobin adsorbed to Cu−DSIDA and Ni−DSIDA monolayers under conditions of constant surface area. Additional experiments performed at constant surface pressure, for various values of surface pressure, will be reported in a future publication.

II. Experimental Section

Materials. The synthesis of DSIDA has been described previously.[17] Myoglobin from horse skeletal muscle (>95% pure) was purchased from Sigma.[31] $CuCl_2$ (99.999%), $NiCl_2$ (99.9%), and D_2O (99.9%) were purchased from Aldrich. The phosphoric acid buffer (pH 7.3) was prepared by dissolving sodium hydrogen phosphate heptahydrate (8.16 g), sodium dihydrogen phosphate monohydrate (1.20 g), and sodium chloride (5.86 g) in 1 L of

(21) The structure of myoglobin was obtained from the protein data bank: 5MBN.

(22) Wuenschell, G. E.; Wen, E.; Todd, R.; Shnek, D.; Arnold, F. H. *J. Chromatogr.* **1991**, *543*, 345.

(23) Sinha, P. C.; Saxena, V. K.; Nigam, N. B.; Srivastava, M. N. *Indian J. Chem.* **1989**, *28A*, 335.

(24) Taunton, H. J.; Toprakcioglu, C.; Fetters, L. J.; Klein, J. *Nature* **1998**, *332*, 712.

(25) Taunton, H. J.; Toprakcioglu, C.; Fetters, L. J.; Klein, J. *Macromolecules* **1990**, *23*, 571.

(26) Weast, R. *CRC Handbook of Chemistry and Physics*, 61st ed.; CRC Press: Boca Raton, 1980.

(27) Losche, M.; Piepenstock, M.; Diederich, A.; Grunewald, T.; Kjaer, K.; Vaknin, D. *Biophys. J.* **1993**, *65*, 2160.

(28) Lee, K. Y. C.; Majewski, J.; Kuhl, T.; Howes, P.; Kjaer, K.; Lipp, M.; Waring, A. J.; Zasadzinski, J. A.; Smith, G. S. *Biophys. J.* **2001**, *81*, 572.

(29) Naumann, C.; Dietrich, C.; Behrisch, A.; Bayerl, T.; Schleicher, M.; Bucknall, D.; Sackman, E. *Biophys. J.* **1996**, *71*, 811.

(30) Maierhofer, A. P.; Bucknall, D. G.; Bayerl, T. M. *Biophys. J.* **2000**, *79*, 1428.

(31) Certain trade names and company products are identified in order to specify adequately the experimental procedure. In no case does such identification imply recommendation or endorsement by the National Institute of Standards and Technology, nor does it imply that the products are necessarily the best for the purpose.

Millipore water (18 MΩ resistivity). Myoglobin was dissolved in 10 mL of the phosphoric acid buffer solution to a concentration of 2 mM. $CuCl_2$ and $NiCl_2$ were dissolved in 10 mL of Millipore water to give a concentration of 6.6 mM.

Methods. Neutron reflection was performed on the NG7 (NIST) and SPEAR (LANL) reflectometers. XR and GIXD experiments were performed on the liquid surface spectrometer at the Advance Photon Source (CMC-CAT, Argonne National Laboratory) using a wavelength of $\lambda = 1.551$ Å. XR experiments were also performed at NIST using a Bruker spectometer equipped with a copper tube source ($\lambda = 1.54$ Å). The NR and XR techniques and analysis methods have been described elsewhere.[32,33] GIXD will be discussed further below. The experiments were performed using a Teflon trough with one movable barrier. The trough was maintained at 20 °C. Addition and circulation of metal ion and protein solutions were accomplished using a peristaltic pump with inlet and outlet tubes placed at each end of the trough. For XR and GIXD, a thick glass plate was introduced just below the meniscus of the subphase, which substantially reduced the surface waves. The trough was contained inside a closed canister to minimize evaporation. The DSIDA lipids were spread onto the subphase from a chloroform solution using a Hamilton microsyringe to a pressure of ∼10 mN/m and then slowly compressed to ∼40 mN/m. Upon addition of $CuCl_2$ or $NiCl_2$ solution to the subphase and circulation, a dramatic drop in surface pressure of >10 mN/m was observed. This was apparently due to the fact that chelation of metal ions reduces the electrostatic charge of the negatively charged IDA headgroup.[14,34] After this drop in surface pressure, the monolayer was compressed further to recover a pressure of 40 mN/m and then myoglobin solution was added to the subphase. The barrier position then remained fixed for the remainder of the run. The amount of $CuCl_2$ added was such as to give a final concentration of 10 μM. The subphase was mixed by operating the circulating pump at a rate of 4 mL/min for 1−3 h (depending on trough volume) prior to the reflectivity measurements. This ensured that the injected metal ions or myoglobin reached the opposite end of the trough, which was visually apparent in the case of myoglobin. The surface pressure was continuously monitored throughout the adsorption process with a Wilhelmy balance. The reflectivity measurements were periodically repeated until no further change was detected. This assessment was on the time scale of several hours, and very slow changes occurring on a much longer time scale would not be detected. For the XR/GIXD runs, special precautions were taken to prevent the intense X-ray beam from damaging the organic monolayer. First, the trough container was continuously purged with helium to minimize oxidative degradation of the organic monolayer in the presence of the X-ray beam. This also reduced the background scattering. Second, the trough was moved by 0.025 mm in the horizontal plane, perpendicular to the incident beam, for each increment of the incident angle. The reproducibility of multiple runs was excellent.

The reflectivity data were analyzed using a least-squares fitting procedure involving multilayer models. Accurate fitting of the NR data required a precise model for the lipid layer. This was determined from the XR data, which were obtained over a much larger range of q_z. The model for the lipid layer and the change in the lipid layer upon protein adsorption were first determined from the XR data, and then this information was imposed in the fits to the NR data. This resulted in a self-consistent analysis of all the data. In fitting the XR data, the electron density within the tail layer was constrained to be consistent with the known area per molecule of 40 Å^2 from the pressure−area isotherm.[14] Since the XR data showed very little change in the lipid headgroup region upon adsorption of myoglobin and since protonated lipids were used, which resulted in little contrast between the protein and the lipid headgroups with NR, when fitting the NR data after adsorption the parameters for the lipid layer were fixed to the values obtained in the absence of myoglobin. Thus, fitting of the NR data in the presence of myoglobin involved only three free parameters: thickness, scattering length density (SLD), and roughness of the protein layer. The range of uncertainty in each fitted parameter was determined by fixing that parameter at various values and allowing the other parameters to vary within physically reasonable limits. Upper and lower limits were determined by the values that led to fits that were unacceptably poor as judged by an increase in χ^2 of 50%.

The reciprocal space GIXD patterns from 2-D ordered crystallites in the monolayers at the interface are comprised of a 2-D array of Bragg rods, which extend parallel to the vertical component, q_z, of the scattering vector $\mathbf{q}$.[35,36] To maximize surface sensitivity for GIXD measurements, the monochromatic X-ray beam was adjusted to strike the surface at an incident grazing angle $\alpha_i \sim 0.1°$, which corresponds to the vertical momentum transfer vector $q_z = 0.85\, q_c$, where $q_c = 0.02176$ Å^{-1} is the critical scattering vector for the total external reflection[37] from a water surface. At this angle the incident wave is totally reflected from the sample, while the refracted wave becomes an evanescent wave traveling along the interface. The intensity of the evanescent wave decreases exponentially with depth, thus enhancing the surface sensitivity and reducing the background scattering from the subphase. The dimensions of the footprint of the incoming X-ray beam on the liquid surface were ∼2 × 50 mm^2. For the collection of diffracted intensities, a vertical one-dimensional position sensitive detector (PSD) with vertical acceptance $0 < q_z < 1.0$ Å^{-1} was used. A Soller collimator was mounted in front of the PSD, defining the horizontal resolution of the detector at $\Delta q_{xy} = 0.009$ Å^{-1}. The scattered intensity was measured by scanning over a range of the horizontal scattering vector component,

$$q_{xy} = (q_x^2 + q_y^2)^{1/2} = \frac{2\pi}{\lambda}[\cos^2(\alpha_i) + \cos^2(\alpha_f) - 2\cos(\alpha_i) \times \cos(\alpha_f)\cos 2\theta_{xy}]^{1/2} \approx (4\pi/\lambda)\sin(2\theta_{xy}/2) \quad (1)$$

where $2\theta_{xy}$ is the angle between the incident and diffracted beam projected onto the horizontal plane, and q_{xy} is the combination of horizontal components q_x and q_y.[38] Such a scan, integrated over all the channels along the q_z direction in the PSD, yields the *Bragg peaks*. Conversely, the scattered intensity recorded in each channel along the PSD, when integrated over the scattering vectors in the horizontal plane across a Bragg peak after background subtraction, produces q_z-resolved scans called the *Bragg rod* profiles. The intensity distribution along a Bragg rod can be analyzed to yield information on the direction and magnitude of the molecular tilt in the crystalline part of the amphiphilic film. In this work we modeled the lipid tail by a cylinder of constant electron density. The adjustable parameters, then, are the tilt angle of the cylinder from vertical, the lateral tilt direction, the length (L_c) of the cylinder (i.e., the length of the part of the molecule that scatters coherently), and the vertical root-mean-square displacement, [σ_z (Debye−Waller factor)] in the crystallites. The horizontal positions (q_{xy}) of the Bragg peaks allow the determination of the spacings $d = 2\pi/q_{xy}$ for the 2-D lattice. The width of the Bragg peaks, corrected for the instrumental broadening, gives the finite size of the crystalline domains in the direction of the reciprocal scattering vector q_{xy} (the 2-D crystalline coherence length L_{xy}).[39] The diffraction peaks were frequently scanned twice. The fact that no loss of intensity was observed confirmed the absence of beam damage.

III. Results

Below we describe data for multiple adsorption runs studied by NR, XR, and GIXD. NR experiments were performed for H_2O and D_2O subphases. The reproducibility

(32) Russell, T. P. *Mater. Sci. Rep.* **1990**, *5*, 171.
(33) Penfold, J.; Thomas, R. K. J. *J. Phys.: Condens. Matter* **1990**, *2*, 1369.
(34) Ishiguro, R., Sasaki, D. Y.; Pacheco, C.; Kurihara, K. *Colloids Surf.* **1999**, *146*, 329.
(35) Als-Nielsen, J.; Kjaer, K. X-ray reflectivity and diffraction studies of liquid surfaces and surfactant monolayers. In *The Proceedings of the NATO Advanced Study Institute, Phase Transitions in Soft Condensed Matter*, Geilo, Norway, April 4−14, 1989, Plenum Publishing Corp.: New York.
(36) Kjaer, K. *Physica B* **1994**, *98*, 100.
(37) Eisenberger, P.; Marra, W. C. *Phys. Rev. Lett.* **1981**, *46*, 1081.
(38) Jensen, T. R.; Kjaer, K. Structural properties and interactions of thin films at the air−liquid interface explored by synchrotron X-ray scattering. In *Novel methods to study interfacial layers;* Miller, R., Ed.; Elsevier: Amsterdam, 2001; Vol. 11, p 205.
(39) Guinier, A. *X-ray Diffraction*, Freeman: San Francisco, 1963.

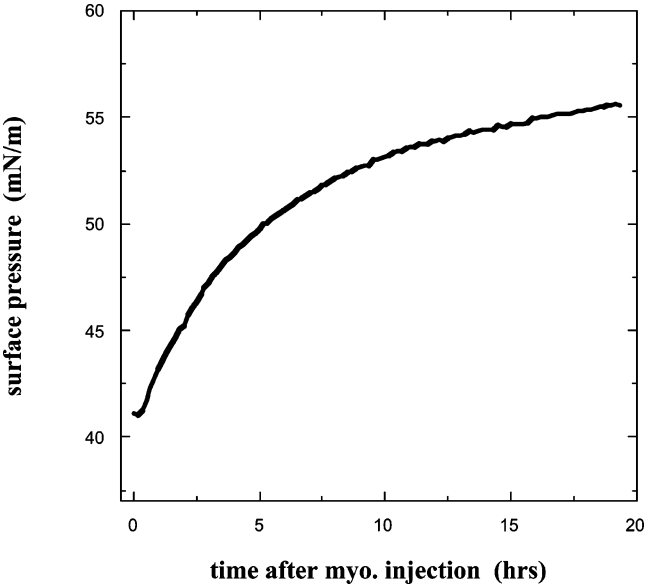

Figure 3. Representative plot of surface pressure versus time after injection of myoglobin for adsorption to Cu-loaded DSIDA from 10 μM bulk myoglobin concentration.

of the reflectivity data was excellent. The adsorbed protein layer could be detected in all the reflectivity experiments, but the contrast was greatest for NR with a subphase of H_2O.

III.1. Surface Pressure. A representative plot of the surface pressure as a function of time after injection of myoglobin (bulk concentration of 10 μM) for the case of adsorption to Cu-loaded DSIDA is shown in Figure 3. The data for adsorption to Ni-loaded DSIDA from a bulk concentration of 50 μM are similar. The pressure continued to gradually increase beyond 20 h after injection, whereas the reflectivity showed little or no change after roughly 12 h. We refer to the structure of the adsorbed layer after 12 h as the "final" state. We acknowledge that further changes may occur on much longer time scales than were probed in this work; however, there is no indication of that in the present data. Below we discuss only the characterization of the layers in the final state. The evolution of the structure of the adsorbed layers with time at the earlier stages will be discussed in a subsequent publication. We note that the form of the pressure−time plot varied considerably with small changes in protocol for both Cu^{2+}- and Ni^{2+}-loaded DSIDA. This will also be discussed further elsewhere. The very slow time scale in Figure 3 indicates that the adsorption process is not diffusion-limited. Presumably, the long time period required for equilibration is due to the ensemble of proteins sampling orientation space until the lowest free energy state is attained, or else may be due to a denaturation process. The ~12 h to reach apparent equilibrium contrasts with an equilibration time of only 2 h for the case of cytochrome *c* adsorbing to mixed monolayers of DMPG and DPPC.[30]

III.2. X-ray Reflectivity. Figure 4a shows representative XR data from the Advanced Photon Source for myoglobin adsorption from 10 μM solution to the DSIDA monolayer loaded with Cu^{2+}. Data are shown prior to addition of myoglobin, and then ~10 h and 10 min after injection of myoglobin, at which point no further changes were detected in the XR curves. The data are plotted as Rq_z^4 to compensate for the q_z^{-4} decay of the Fresnel law and thus more clearly reveal the changes that occur upon protein adsorption. The characteristics of the adsorbed protein layer impact the reflectivity mainly from $q_z = 0.025$ to 0.13 Å^{-1}. This region is shown in an expanded view in Figure 4b. Variations in reflectivity at higher q_z values derive mainly from changes in the characteristics of the lipid film. Variations in reflectivity at higher q_z values derive mainly from changes in the characteristics of the lipid film. The magnitude of the change in the range $q_z = 0.025-0.13$ Å^{-1} upon adsorption of myoglobin to the final state was very reproducible for multiple runs. The magnitude of the change in the range of $q_z = 0.025-0.13$ Å^{-1} upon adsorption of myoglobin to the final state was very reproducible for multiple runs.

Best-fit scattering length density profiles for the curves of Figure 4a are shown in Figure 4c. The origin of the distance scale is placed at the interface of the lipid headgroup with the protein or subphase. We note that since the portion of the curve that reflects the structure of the adsorpted protein layer falls at low q_z values, this portion can easily be obtained with an in-house X-ray source. Several such runs were performed in addition to the data shown in Figure 4a. In the analysis of the data for these runs, the characteristics of the lipid layer were fixed at the values obtained from the data in Figure 4a involving a higher q_z range. One XR run was performed with 10 μM myoglobin and Cu-loaded DSIDA but using D_2O as the subphase (data not shown) in order to aid in the interpretation of the neutron data discussed below.

III.3. Neutron Reflectivity. NR data for myoglobin adsorption from 10 μM solution to Cu-loaded DSIDA in an H_2O subphase is shown in Figure 5a. Reflectivity data are shown for the DSIDA monolayer with chelated Cu^{2+} prior to addition of myoglobin and then after addition of myoglobin and attainment of the final state. Again, excellent reproducibility was obtained for multiple runs. The best-fit SLD profile is shown in Figure 5b. The variation in χ^2 with the value of thickness imposed in the fitting is shown in the inset to Figure 5a. This plot was used to determine the uncertainty in the thickness.

Another experiment was performed with an H_2O subphase using conditions identical to that for the data in Figure 5a but without addition of metal ions. No change in reflectivity occurred upon injection of myoglobin in that case (data not shown). This is consistent with the loss of specific histidine−Cu−IDA interactions and the lack of nonspecific interactions between the charge-neutral myoglobin and the negatively charged DSIDA.

NR data for myoglobin adsorption from 10 μM solution to Cu-loaded DSIDA in a D_2O subphase are shown in Figure 6a. Reflectivity data are shown for the DSIDA monolayer with chelated Cu^{2+} prior to addition of myoglobin and then after addition of myoglobin and attainment of the final state. The best-fit SLD profile is shown in Figure 6b. The contrast was lower than with the H_2O subphase, but the reflectivity was much higher, requiring a shorter counting time to obtain adequate statistics. This, and a lower background level, led to a much larger q_z range in D_2O than in H_2O.

Figure 7 shows reflectivity data for adsorption of myoglobin to Cu-loaded DSIDA with a subphase concentration of 0.1 μM. On the basis of the adsorption isotherm data of Shnek et al.,[14] this concentration should be far below the concentration at which the plateau in the adsorption isotherm is obtained. Indeed, the adsorbed amount is far less than for the case of adsorption to Cu−IDA at 10 μM myoglobin.

NR data for myoglobin adsorption from 50 and 10 μM solution to Ni-loaded DSIDA in H_2O subphase are shown in Figure 8a and Figure 8b, respectively. In each case, reflectivity data are shown prior to addition of myoglobin, and also after addition of myoglobin and attainment of

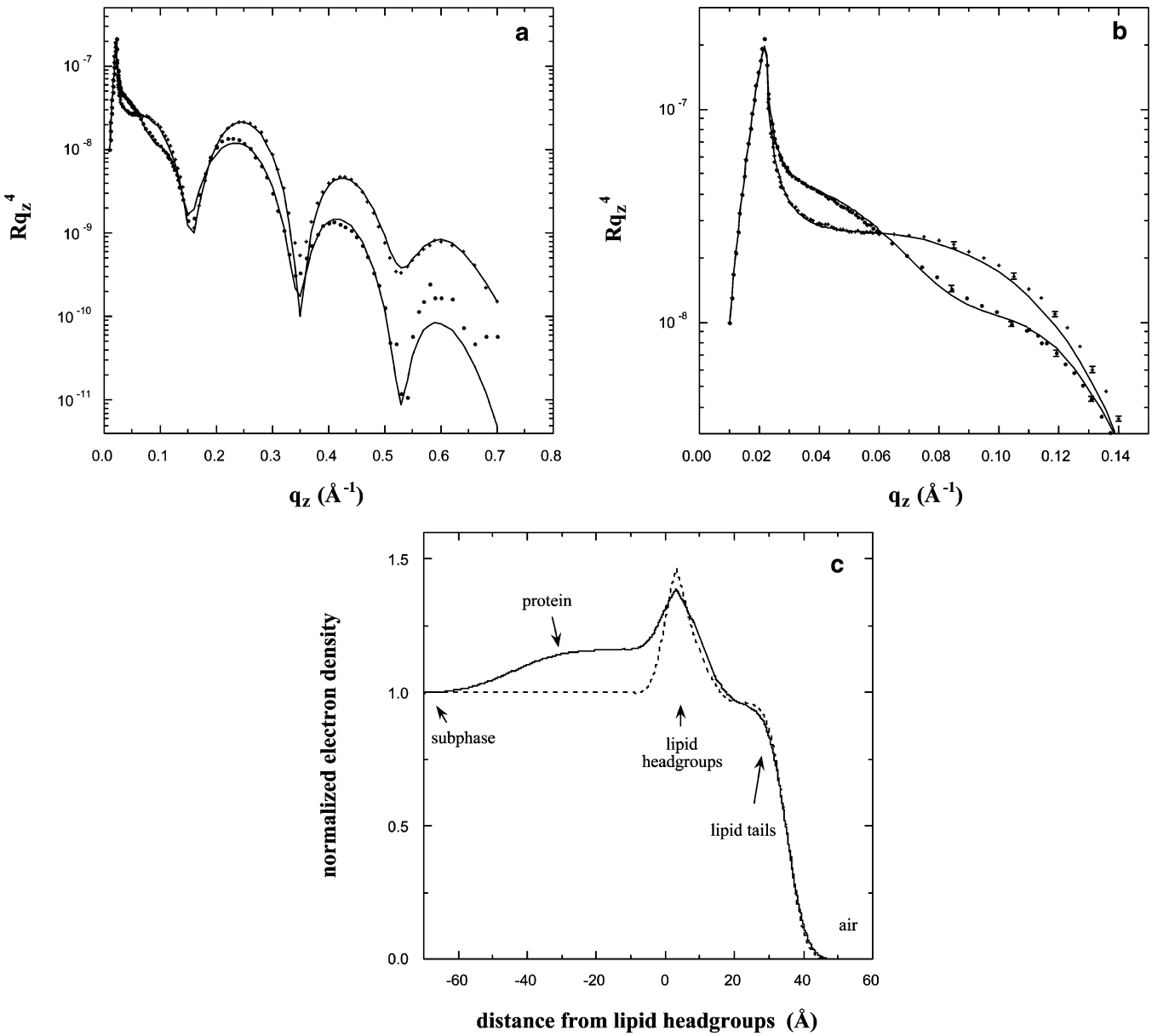

Figure 4. (a) X-ray reflectivity data obtained for adsorption of myoglobin to Cu^{2+}-loaded DSIDA from a solution concentration of 10 μM in H_2O subphase. Data are shown prior to injecting myoglobin (+) and 10 h and 10 min after injecting myoglobin (●). The error bars are smaller than the size of the symbols. (b) Expanded view of the lower q range where protein layer structure impacts the reflectivity data. (c) Normalized electron density profiles corresponding to the best-fit curves in a and b: prior to injecting myoglobin (dashed line) and 10 h and 10 min after injecting myoglobin (solid line).

the final state. The data in Figure 8 reveal a strong dependence of the adsorbed amount on the bulk myoglobin concentration over this concentration range. The data in Figure 8b indicate that the amount adsorbed to Ni-loaded DSIDA at 10 μM myoglobin is comparable to that obtained for adsorption to Cu-loaded DSIDA at 0.1 μM myoglobin. Note, however, that the dimensions of the layers are quite different for these two cases. This can be seen by the fact that for adsorption to Cu-loaded DSIDA at 0.1 μM myoglobin the reflectivity remains above that for the initial lipid film up to $q_z = 0.10$ Å^{-1} (Figure 7), but for adsorption to Ni-loaded DSIDA at 10 μM myoglobin the reflectivity falls below that for the initial lipid film at values above $q_z \sim 0.07$ Å^{-1} (Figure 8b).

III.4. Grazing Incidence X-ray Diffraction (GIXD). GIXD measurements provide in-plane structural information on the crystalline, diffracting portion of the monolayer. Diffraction data (Bragg peaks and Bragg rods) for the DSIDA monolayer with Cu^{2+} ions and also after injection of myoglobin are shown in Figure 9. The structural parameters from the fitting analysis are summarized in Table 1. Figure 9a shows the Bragg peak as a function of the horizontal scattering vector component, q_{xy}, for a pure DSIDA monolayer and also at 3.8 and 14.2 h after injecting myoglobin into the subphase. Only one in-plane Bragg peak $\{1, 0\}$[40] was observed which occurred at $q_{xy} = 1.52$ Å^{-1}, indicating the existence of 2-D crystallites with a hexagonal unit cell with d spacing $a_h = 4.77$ Å and area per DSIDA molecule = 39.4 Å^2. Comparing the Bragg peak positions before and after injecting myoglobin demonstrates that adsorption of myoglobin does not interfere with the unit cell dimensions of the ordered DSIDA molecules. However, there are distinct differences in the relative intensities of the Bragg peaks and their width at half-maximum height.

(40) In our notation, $\{1, 0\}$ indicates six coinciding reflections $\{h,k\} = \{(1, 0),(0, 1),(\bar{1}, 1),(\bar{1}, 0),(0, \bar{1}),(1, \bar{1})\}$.

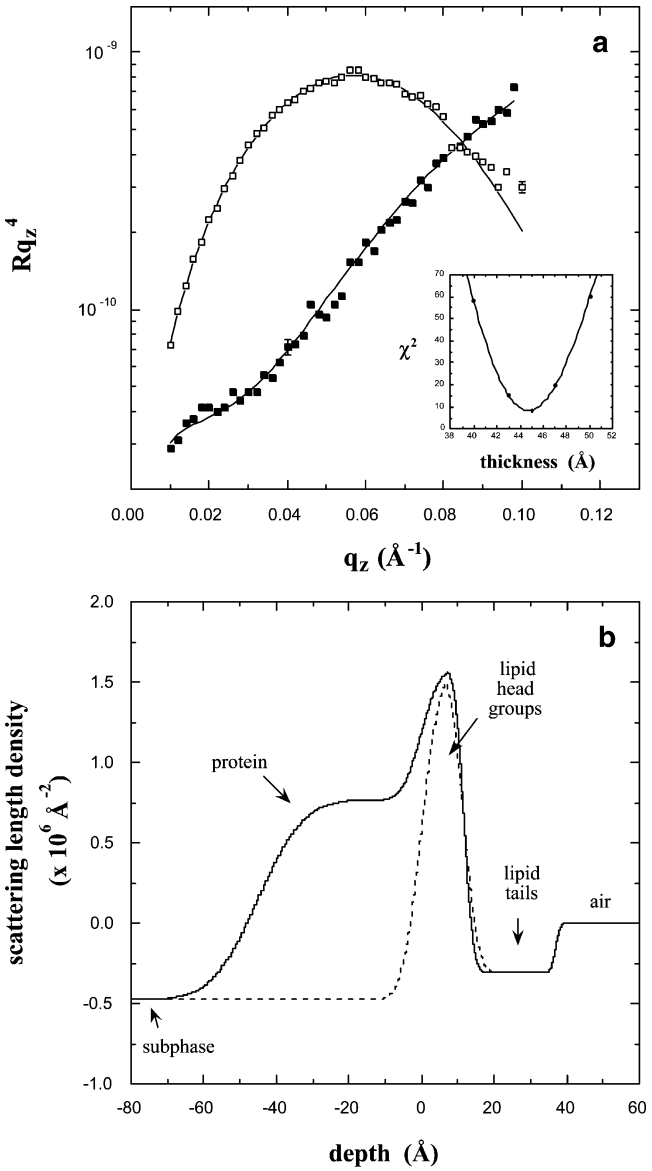

Figure 5. (a) Neutron reflectivity data obtained for adsorption of myoglobin to Cu^{2+}-loaded DSIDA from a solution concentration of 10 μM in H_2O subphase. Data are shown prior to injecting myoglobin (■) and 12.7 h after injection (□). A χ^2 analysis of the thickness is shown in the inset. (b) SLD profiles corresponding to the best-fit curves through the data in (a): prior to injecting myoglobin (dashed line) and 12.7 h after injecting myoglobin (solid line).

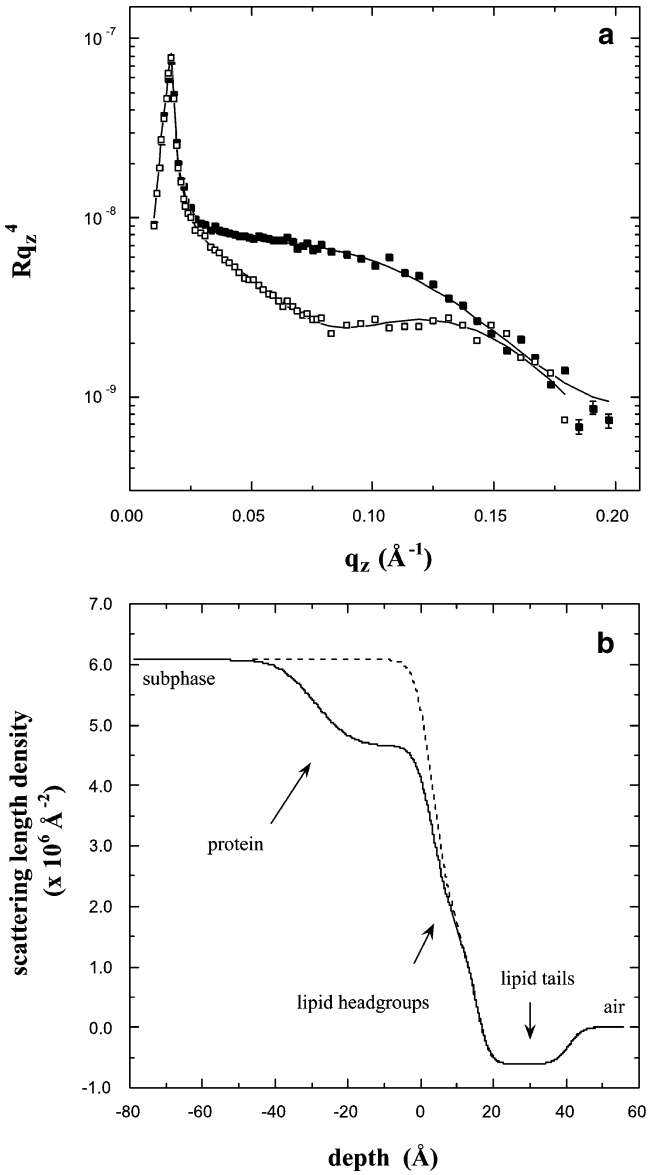

Figure 6. (a) Neutron reflectivity data obtained for adsorption of myoglobin to Cu^{2+}-loaded DSIDA from a solution concentration of 10 μM in D_2O subphase. Data are shown prior to injection of myoglobin (■) and 14.9 h after injection (□). (b) SLD profiles corresponding to the best-fit curves through the data: prior to injecting myoglobin (dashed line) and 14.9 h after injecting myoglobin (solid line).

The corresponding full width at half-maximum height (fwhm) of the three peaks are $\text{fwhm}_{\text{meas}}(q_{xy}) = 0.0148$ Å^{-1} (DSIDA + Cu^{2+}), $\text{fwhm}_{\text{meas}}(q_{xy}) = 0.0169$ Å^{-1} (3.8 h after injecting myoglobin), and $\text{fwhm}_{\text{meas}}(q_{xy}) = 0.0130$ Å^{-1} (14.2 h after injecting myoglobin), all of which exceed the instrumental broadening of $\text{fwhm}_{\text{instrum}}(q_{xy}) = 0.009$ Å^{-1}. The intrinsic fwhm can be obtained using the equation

$$\text{fwhm}_{\text{intrinsic}}(q_{xy}) = [\text{fwhm}_{\text{meas}}(q_{xy})^2 - \text{fwhm}_{\text{instrum}}(q_{xy})^2]^{1/2} \quad (2)$$

A simple model assumes that the monolayer consists of 2-D crystallites that are perfect and have a finite average size L_{xy}, the *coherence length*. Using the Scherrer formula,[39] the coherence length in the crystallographic directions $L_{xy} \approx 0.9[2\pi/\text{fwhm}_{\text{intrinsic}}(q_{xy})]$ can be calculated for the {1,0} Bragg peak (L_{10}). We find the corresponding coherence lengths for the peaks to be 480 Å (pure DSIDA), 400 Å (DSIDA/myoglobin after 3.8 h), and 600 Å (DSIDA/myoglobin after 14.2 h), respectively. Accordingly, the integrated intensity of the Bragg peaks are in the following proportion: 1:0.72:2.2. This indicates that despite the lack of change in the unit cell dimensions of the DSIDA tails, in the initial stages of myoglobin interaction with the DSIDA monolayer the size of the correlated DSIDA islands decreases. In the latter stages, as the DSIDA monolayer approaches equilibrium, better 2-D ordering occurs in the form of larger domains.

The Bragg rod profile integrated over the q_{xy} region corresponding to the {1,0} reflection is shown in Figure 9b for the monolayer at 14.2 h after injecting myoglobin. All other Bragg rod scans were nearly identical in shape to that shown in Figure 9b. The {1,0} Bragg rod achieves its maximum intensity at $q_z \sim 0$ Å^{-1}, indicating that the molecular axis of DSIDA lies perpendicular to the surface of the subphase. We analyzed the {1,0} Bragg rod intensity profiles by approximating the fatty DSIDA tail by a

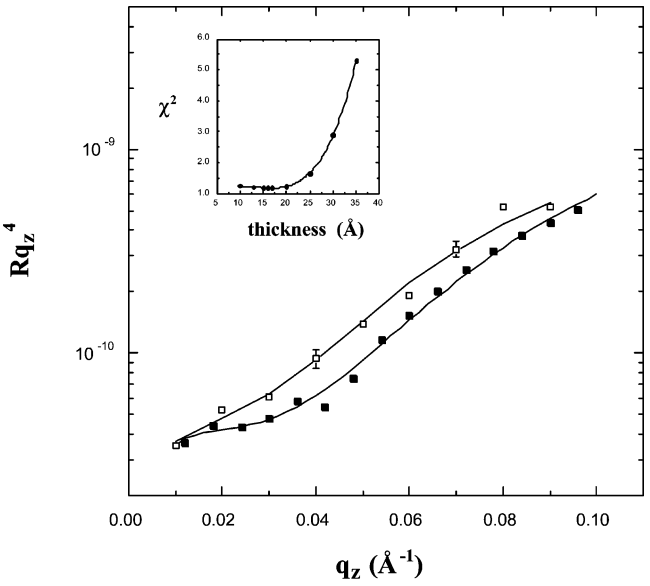

Figure 7. (a) Neutron reflectivity data obtained for adsorption of myoglobin to Cu^{2+}-loaded DSIDA from a solution concentration of 0.1 μM in H_2O subphase. Data are shown prior to injection of myoglobin (■) and 19.0 h after injection (□). Results of a χ^2 analysis of the thickness is shown in the inset.

cylinder with a constant electron density.[35] Our analysis shows that in all cases the DSIDA molecule has a tilt of approximately 0.0° from the surface normal. The effective coherently scattering length of the DSIDA molecule, L_c, is 20.8 ±0.2 Å, which is in good agreement with the hydrocarbon tails in all-trans configuration.

In all the investigated cases no lower order reflections were observable, indicating that despite being bound to the alkyl chains, the DSIDA headgroups were too disordered to be observed by GIXD. Additionally, the scan performed at 14.2 h after injection was extended down to $q_{xy} = 0.5$ Å^{-1} to check for the presence of larger crystalline structures that might arise from the layer of adsorbed protein. No diffraction peaks were observed at this low q_{xy}. This q_{xy} range coincides with that for the higher order peaks for myoglobin in crystalline form. Even lower q_{xy} values would be required to observe the primary peaks. Nevertheless, the absence of peaks over this q_{xy} range strongly suggests that there is no crystalline structure within the layer of adsorbed protein. This is consistent with the fact that 2-D protein crystals have only been observed to form underneath lipids in the amorphous phase.[5−7]

IV. Discussion

Insight into the orientation and conformation of the adsorbed protein can be obtained through precise measurements of the thickness and segment volume fraction of the layer. The thickness data in the final state for the various runs are given in Table 2. We consider first the case of adsorption of myoglobin to Cu-loaded DSIDA from 10 μM solution. The values from XR for both subphases and from NR in H_2O subphase are in good agreement. The values from NR in D_2O subphase are distinctly lower than those for the other runs, with the difference lying outside the statistical uncertainty in the fitting. This will be discussed further below. Notice that the uncertainty is smallest for NR in the H_2O subphase, larger for NR in the D_2O subphase, and largest for XR. This results from differences in the contrast. The thickness values obtained from the XR runs and the NR runs with H_2O are comparable to the larger dimensions of myoglobin (44 Å × 44 Å × 25 Å) and thus are consistent with adsorption of the

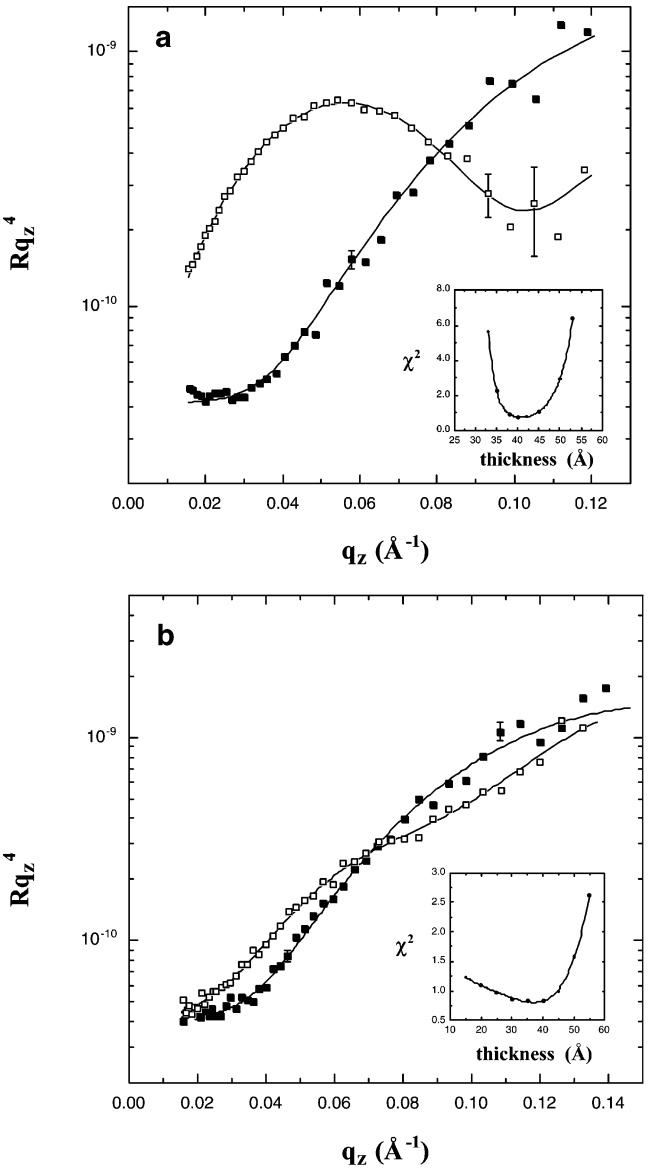

Figure 8. (a) Neutron reflectivity data obtained for adsorption of myoglobin to Ni^{2+}-loaded DSIDA from a solution concentration of 50 μM in H_2O subphase. Data are shown prior to injection of myoglobin (■) and 17 h after injection (□). (b) Neutron reflectivity data obtained for adsorption of myoglobin to Ni^{2+}-loaded DSIDA from a solution concentration of 10 μM in H_2O subphase. Data are shown prior to injection of myoglobin (■) and 14 h after injection (□).

disk-shaped protein in an end-on orientation at high packing density. We note that the thickness of the adsorbed protein layers in the present work are much smaller than we reported previously for myoglobin adsorbed to a mixed monolayer containing a fluid-phase metal-chelating lipid and d_{62}-2-dipalmitoyl-*sn*-glycero-3-phosphocholine (87 Å).[41] This requires further study but appears to suggest that the structure of the adsorbed layer is affected by the phase state of the membrane to which it is adsorbing.

An absolute determination of the volume fraction and the melt density of myoglobin could be obtained from the magnitude of the change in reflectivity for the XR runs and the NR runs in the H_2O subphase. The following equations describe the neutron SLD (b/v) and the real part of the X-ray refractive index (δ) for the mixed layer of protein and subphase that determine the neutron and X-ray refractive in the H_2O subphase:

Table 1. Parameters from GIXD for DSIDA before and after Myoglobin Adsorption

composition	surface pressure, mN/m	area per DSIDA molecule, Å^2	unit cell	relative intensity	a_h, Å	$L_{10} \pm 20$, Å	$L_c \pm 0.2$, Å	tilt direction	tilt angle $\pm 0.9°$, deg
DSIDA	40.4	39.4	hexagonal	1	4.77	480	20.8	n/a	0.0
DSIDA/myo, 3.8 h	47.6	39.4	hexagonal	0.72	4.77	400	20.8	n/a	0.0
DSIDA/myo, 14.2 h	54.0	39.4	hexagonal	2.2	4.77	600	20.8	n/a	0.0

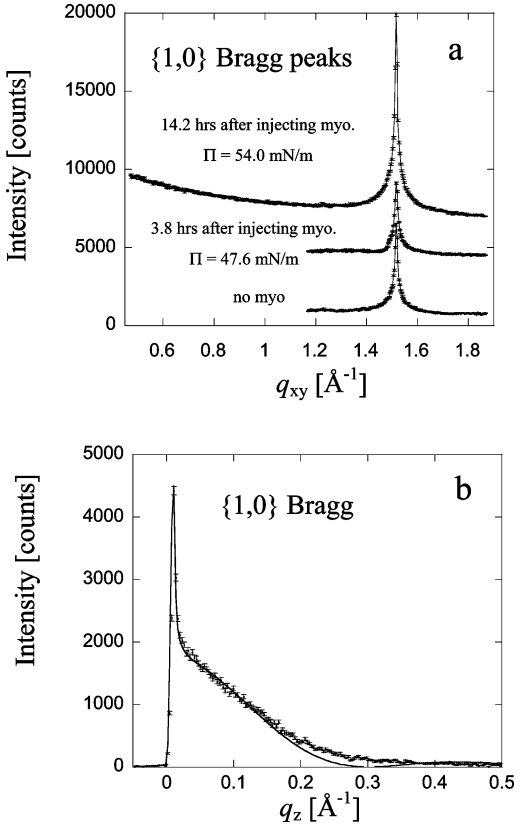

Figure 9. (a) Bragg peaks from GIXD for films of Cu-loaded DSIDA prior to injecting myoglobin and at 3.8 and 14.2 h after injecting myoglobin. For clarity, the data have been offset vertically. The single GIXD Bragg peak {1,0} (hexagonal lattice) indicates a hexagonal packing of the tails in a 2-D unit cell lattice with parameters $a_h = 4.77$ Å. (b) Bragg rod profile for {1,0} Bragg peak measured at 14.9 h after injecting myoglobin. The Bragg rod from this scan was identical in shape to that obtained prior to injecting myoglobin. The rod was fitted (—) by approximating the coherently scattering part of the acyl chain by a cylinder of constant electron density. The sharp peak at $q_z = 0.01$ Å^{-1} is the so-called *Yoneda−Vineyard* peak,[45] which arises from the interference between X-rays diffracted up into the Bragg rod and X-rays diffracted down and then reflected up by the interface. The molecular packing parameters obtained from the fitting analysis of the Bragg peak and Bragg rod are listed in Table 1. Despite the dense layer of adsorbed myoglobin driven by the strong interaction between Cu^{2+} and the histidine residues, little change is observed in the structure of the DSIDA film.

$$\text{(NR)} \quad b/v = \phi_{myo}(b/v)_{myo,H} + (1 - \phi)(b/v)_{sub(H)} \quad (3)$$

$$\text{(XR)} \quad \delta = \phi_{myo}\delta_{myo} + (1 - \phi)\delta_{sub} \quad (4)$$

$$(b/v)_{myo,H} = (1.35 \times 10^{-6}\ \text{Å}^{-2})\rho_{myo} \quad (5)$$

$$\delta_{myo} = (3.48 \times 10^{-6})\rho_{myo} \quad (\text{at } \lambda = 1.551\ \text{Å}) \quad (6)$$

where ϕ_{myo} and ρ_{myo} are the volume fraction and melt density of peptide segments in the adsorbed layer, respectively. These two measurements combined thus provide enough information to determine the absolute peptide segment volume fraction within the adsorbed layer and the melt density of myoglobin. The b/v values for the protein layer from the three NR runs and the δ values for the protein layer from the two XR runs result in an average volume fraction of 0.55 ± 0.05 and a melt density of 1.43 g/cm$^3 \pm 0.04$. The value for the melt density of myoglobin compares favorably with the average value of the density of the amino acids comprising the protein.[42] However, the measured average volume fraction is substantially greater than the average volume fraction of 0.44 calculated from the dimensions of myoglobin obtained from the crystal structure.[43] This may indicate that the strong attraction with the surface causes denaturation. The data for thickness and segment volume fraction correspond to an adsorbed amount of 11.1 molecules/(100 Å)^2.

Table 2. Thickness Values for the Adsorbed Layer of Myoglobin from the Fitting Analysis

metal ion	myo concn, μM	exptl method	subphase	thickness, Å
Cu^{2+}	10	XR	H_2O	43.3 ± 5 (run 1)
Cu^{2+}	10	XR	H_2O	44.2 ± 5 (run 2)
Cu^{2+}	10	XR	D_2O	42.5 ± 5
Cu^{2+}	10	NR	H_2O	44.8 ± 1.5 (run 1)
Cu^{2+}	10	NR	H_2O	42.5 ± 2.0 (run 2)
Cu^{2+}	10	NR	H_2O	41.0 ± 1.5 (run 3)
Cu^{2+}	10	NR	D_2O	32.6 ± 3.5 (run 1)
Cu^{2+}	10	NR	D_2O	36.0 ± 4.0 (run 2)
Cu^{2+}	0.1	NR	H_2O	≤ 25
Ni^{2+}	10	NR	H_2O	38 ± 9
Ni^{2+}	50	NR	H_2O	41 ± 4.5

Thus, the data in H_2O for 10 μM myoglobin are consistent with a monolayer of myoglobin in the native state in an end-on orientation but at a packing density greater than in the crystalline state. The GIXD and XR data indicate that, other than modest changes in the size of the correlated domains, the phase state of the lipid film is not affected by the adsorption of myoglobin. There is no evidence in the GIXD or XR for insertion of peptide segments into the lipid tail region. A sensitivity analysis indicated that a decrease in the in-plane average density of the tail layer of >2% would be detectable by XR. We note that for the XR data in Figure 4a, the fits indicated a small decrease in the electron density of the headgroup region upon adsorption of myoglobin. This may indicate

(41) Kent, M. S.; Yim, H.; Sasaki, D.; Majewski, J.; Smith, G. S.; Shin, K.; Satija, S.; Ocko, B. M. *Langmuir* **2002**, *18*, 3754. Note that the amino acid volume fraction calculated in that paper assumed a melt density of 0.80 for myoglobin. Since the melt density of myoglobin was determined to be 1.43 from the present data, the values in Figure 4 of the above paper should be multiplied by 1.43/0.80, giving a maximum value of 0.20 at the surface rather than 0.11. This value is still far less than 0.55 ± 0.05 as observed in the present work and is also less than the value of 0.44 expected for full coverage in the native state.

(42) The bulk density values for only 12 of the amino acids (Gly, Leu, Ser, Asp, Glu, Met, Val, Asn, Ala, Arg, Tyr) could be found in the literature. Using these values and the number of each amino acid present in myoglobin, a weight average value of 1.44 g/cm^3 was calculated.

(43) This estimate was calculated as $(M/N_A\rho)/(44\ \text{Å} \times 44\ \text{Å} \times 25\ \text{Å})$, using a molecular weight (M) of 18 400 and a melt density (ρ) of 1.43 g/cm^3. N_A is Avogadro's number.

insertion of some peptide segments into that region. Such an effect could not be detected in the NR study due to the absence of contrast with protonated lipids, but it might be detectable in NR if deuterated lipids were used.[29]

Determining ϕ_{myo} from the NR data in the D_2O subphase is complicated by the possibility of deuterium exchange in myoglobin. de Jongh et al. studied the exchange of labile protons for deuterons in myoglobin exposed to D_2O by IR.[44] They reported that 100% exchange of the amide protons from the disordered regions occurred within 5 h, and 60% exchange of the amide protons from the helical regions occurred within 13 h. Our solutions were prepared at least 1 day prior to use, so we assume 100% exchange has occurred. The peptide segments containing labile protons are not distributed uniformly but occur more typically on the outer surface of the protein exposed to the aqueous solvent. Thus, exchange of D for H will lead to reduced contrast at the outer regions of the protein and perhaps a profile for an adsorbed layer composed of two slabs. We estimate that exchange could lead to a difference in SLD between inner and outer regions of as much as 4.7×10^{-6} Å^{-2} (inner region) and 5.7×10^{-6} Å^{-2} (outer region). However, it is not possible to distinguish between a single layer and a profile composed of two slabs in the present data, because the roughness between the protein layer and the subphase is comparable in dimension to the thickness of the outer layer. Assuming 100% exchange of the labile protons and using a single layer profile, the average segment volume fraction is 0.49 and 0.42 for NR runs 1 and 2 in D_2O. These values agree well with the value of 0.46 from XR in D_2O, but they are well below the value of 0.55 ± 0.05 determined from the data for XR and NR in H_2O. Thus, we conclude that the adsorbed amount is slightly lower in D_2O than in H_2O for measurements obtained on a similar time scale. We note that since it is very difficult to determine the precise final state due to the very slow approach to equilibrium in the later stages of adsorption experienced by these systems, the difference in adsorbed amount may correspond to a slightly different kinetics in the later stages of adsorption in H_2O and D_2O. Since the thickness obtained by XR in D_2O is comparable to that obtained by XR and NR in H_2O, we attribute the slightly reduced thickness obtained by NR in D_2O to loss of contrast at the outer edges resulting from exchange of D for H.

Next we consider the case of adsorption to Cu-loaded DSIDA from 0.10 μM solution shown in Figure 7. The thickness of the layer is $\leq$25 Å. The plot of χ^2 versus thickness is shown in the inset. For any thickness in the range of 10−25 Å, the thickness and corresponding best-fit segment volume fraction correspond to an adsorbed amount of ~1.3 molecules/(100 Å)^2, which is about $^1/_{10}$ of the value obtained for adsorption from 10 μM solution. This much lower adsorbed amount is as expected, based on the adsorption isotherm reported by Shnek et al.[14] However, it is interesting to note that the thickness of $\leq$25 Å is substantially less than the thickness of the layer adsorbed from 10 μM solution. One possible interpretation is that the orientation changes with packing density. Alternatively, the protein may denature upon adsorption and the increase in thickness with adsorbed amount may be due to the build up of the denatured layer as more proteins adsorb to the remaining available sites. An increase in pressure of 7.4 mN/m was observed after ~12 h, far less than the ~14 mN/m observed in the case of adsorption from 10 μM solution. Since the adsorbed amount corresponds to far less than a completed monolayer, the 7.4 mN/m must arise from interactions between adsorbed protein and the lipid film rather than from interactions among the adsorbed protein molecules. We reiterate that there is no evidence in XR for penetration of segments into the lipid tail region. However, a decrease in the in-plane average density of the tail layer of 2% or less would be undetectable by XR. Therefore, a low level of insertion might indeed occur, perhaps at the disordered regions between crystalline domains. The pressure might also arise from penetration of segments into the headgroup region or from the constraint of having the DSIDA headgroups match up precisely with the histidine units on the protein surface.

Finally, we consider the case of adsorption to Ni-loaded DSIDA. The data for adsorption from 50 μM solution shown in Figure 8a corresponds to a layer thickness of 41.0 ± 4.5 Å and an average segment volume fraction of 0.52. The thickness and volume fraction correspond to an adsorbed amount of 10.0 molecules/(100 Å)^2, which is comparable to the value obtained for adsorption to Cu-loaded DSIDA from 10 μM solution. The data for adsorption from 10 μM solution shown in Figure 8b corresponds to a layer thickness of 38 ± 9 Å and an average segment volume fraction of 0.12. The thickness and volume fraction correspond to an adsorbed amount of 2.1 molecules/(100 Å)^2, which is comparable to the value obtained for adsorption to Cu-loaded DSIDA from 0.1 μM solution. However, the thickness of 38 ± 9 Å is substantially greater than that obtained for adsorption to Cu-loaded DSIDA from 0.1 μM solution ($<$25 Å). Thus, whereas the adsorbed amount is comparable for the two cases (adsorption to Ni-loaded DSIDA from 10 μM solution and adsorption to Cu-loaded DSIDA from 0.1 μM), the orientation or conformation of the adsorbed myoglobin is substantially different. Presumably, this is due to the very different energies for the individual binding interactions in the two cases. A stronger interaction energy per site may cause the myoglobin to be adsorbed in an orientation that strains it in order to access more binding sites per molecule. Such a strained orientation/conformation may not be supported by the weaker interactions in the case of Ni^{2+}. Alternatively, the protein may denature upon adsorption to a greater extent with Cu-loaded DSIDA than with Ni-loaded DSIDA. We note that an increase in pressure of 6.3 mN/m was observed in the case of adsorption to Ni^{2+}-loaded DSIDA at 10 μM myoglobin, and again this must be due to an increased pressure within the lipid film upon protein adsorption rather than from interactions among the adsorbed protein molecules, since the protein coverage is much less than a completed monolayer.

The data for protein coverage and pressure increase in the present work can be compared with the data from previous studies of proteins adsorbing to lipid monolayers. The adsorption of cytochrome *c* to mixed monolayers of DPPC and DMPG through nonspecific electrostatic interactions was examined at subphase concentrations ranging from 0.4 to 0.7 μM. This resulted in coverages ranging from 20−48% of full coverage for lipid compositions ranging from 70:30 to 20:80 of DPPC and DMPG and for both liquid-expanded and liquid-condensed phases.[30] The pressure increase upon adsorption ranged from 3 to 8 mN/m. The protein coverage and pressure increase are thus comparable to the present observations for myoglobin adsorption to Cu-loaded DSIDA from 0.1 μM solution and to Ni-loaded DSIDA from 10 μM solution. The adsorption of hisactophilin (HIS) from 0.1 μM solution to mixed monolayers of DMPC and DMPG was also largely

(44) de Jongh, H. H. J.; Goormaghtigh, E.; Ruysschaert, J.-M. *Biochemistry* **1997**, *36*, 13603.
(45) Vineyard, G. *Phys. Rev. B* **1982**, *26*, 4146.

electrostatic in origin and resulted in protein coverages ranging from 0.04 to 0.35 of full coverage as the fraction of charged lipid increased from 0 to 0.5,[29] again comparable to the present observations for myoglobin adsorption to Cu-loaded DSIDA from 0.1 μM solution and to Ni-loaded DSIDA from 10 μM solution. On the other hand, Losche et al. reported nearly full coverage of streptavidin adsorbing from a subphase concentration of 0.02 μM to biotinylated lipid films at an initial surface pressure of 3 mN/m.[27] This is comparable to the present results for myoglobin adsorption to Cu-loaded DSIDA from 10 μM solution or to Ni-loaded DSIDA from 50 μM solution and demonstrates the very strong binding affinity of the streptavidin/biotin system.

Summary

Neutron and X-ray reflectivity and GIXD have been used to study the structure of myoglobin adsorbed to metal-chelating lipid monolayers noninvasively and in situ. The protein layer could be detected with both XR and NR; however, the contrast was most favorable with NR and an H_2O subphase. In all cases, the volume fraction profile of amino acid segments could be modeled by a single layer with a smooth transition region to the subphase. The adsorption was studied at a fixed area per lipid molecule ($\sim$40 Å^2) at an initial pressure of 40 mN/m. After $\sim$12 h little further change in reflectivity was detected, although the surface pressure continued to slowly increase. For Cu-loaded DSIDA, the adsorbed layer was examined for bulk myoglobin concentrations of 10 and 0.1 μM. The former is well onto the adsorption plateau, while the latter is far below the adsorption plateau. The layer thickness was very different for these two cases, with the value at the higher concentration corresponding to the larger dimensions of myoglobin and the thickness obtained at the lower concentration comparable to the smaller dimension. This may suggest that the orientation of the adsorbed protein changes as the packing density increases. However, the average segment volume fraction in the adsorbed layer for 10 μM myoglobin was substantially greater than that estimated for a completed monolayer from the crystallographic data. This suggests an alternative interpretation based on denaturation. The layer thickness and segment volume fraction obtained in the D_2O subphase at 10 μM were both lower than that obtained in the H_2O subphase. Since the thickness in D_2O as measured by XR was comparable to the values obtained by XR and NR in H_2O, the lower thickness values in D_2O by NR are assumed to be due to H/D exchange.

The adsorbed layer structure was also examined at 50 and 10 μM in H_2O for DSIDA monolayers loaded with Ni^{2+}. At 10 μM the adsorption was far lower with Ni^{2+} than with Cu^{2+}, resulting in an average segment volume fraction about one-fourth of that estimated for a full monolayer in the native state. This was as expected, since the binding interaction of histidine is known to be much weaker for Ni−IDA than for Cu−IDA. Interestingly, whereas the adsorbed amounts were comparable for adsorption to Cu^{2+}-loaded monolayers from 0.1 μM solution and adsorption to Ni^{2+}-loaded monolayers from 10 μM, the layer thickness was much greater in the later case. This suggests either that the preferred orientation at low coverage is different for the cases of Ni^{2+} and Cu^{2+} or else that a greater extent of denaturation occurs for Cu-loaded DSIDA. Either interpretation can be explained by the much stronger binding interaction between histidine and Cu−IDA. We expect that a detailed examination of the time evolution of the adsorbed layer structure will distinguish between these two interpretations. The thickness of the layer adsorbed to Ni−IDA at 50 μM myoglobin was comparable to that adsorbed to Cu-IDA at 10 μM.

We note that there was no evidence for crystallinity in the protein layer. This supports the denaturation interpretation but could also be due to the restricted mobility of the lipids in crystalline phase. Despite the dense layer of adsorbed myoglobin at 10 μM driven by the strong interaction between Cu^{2+} and the histidine residues, little change was observed in the structure of the DSIDA film for the present conditions, where the area per lipid molecule was maintained constant. There was no direct evidence in either GIXD or XR for insertion of peptide segments into the lipid tail region. However, a very low level of insertion might exist in the disordered regions between the crystalline lipid domains that would not be detectable by either GIXD or XR and could explain the increase in pressure observed. Only a very slight increase in roughness and modest changes in the size of the correlated lipid domains were detected upon adsorption.

Acknowledgment. This research was supported in part by the Division of Materials Science and Engineering in the Department of Energy Office of Basic Energy Sciences. Sandia is a multiprogram laboratory operated by Sandia Corp., a Lockheed Martin company, for the United States Department of Energy under contract DE-AC04-94AL85000. We acknowledge the support of the National Institute of Standards and Technology, U.S. Department of Commerce, in providing the neutron research facilities used in this work. This work has also benefited from the use of the Los Alamos Neutron Science Center at the Los Alamos National Laboratory. This facility is funded by the U.S. Department of Energy under contract W-7405-ENG-36. Use of the Advanced Photon Source (CMC-CAT) was supported by the U.S. Department of Energy, Office of Science, Office of Basic Energy Sciences, under contract no. W-31-109-Eng-38.

LA036207Y